Proceedings of the 1996 IEEE
International Conference on Robotics and Automation
Minneapolis, Minnesota - April 1996

Simulation of Contact Using a Nonlinear Damping Model

Duane W. Marhefka and David E. Orin

Department of Electrical Engineering
The Ohio State University
Columbus, OH 43210

Abstract

In this paper, a simple nonlinear contact model is presented for use in computer simulation. The nonlinear model is shown to maintain the computational simplicity of the linear model while addressing many of its deficiencies. One such advantage is that contact forces vary continuously over time. A new phase plane solution for the nonlinear model is obtained which reveals many previously unnoted properties. These include proper variation of the coefficient of restitution with impact velocity over a wide range of impact velocities, independence of model parameters, and lack of tensile (sticking) forces in simple impacts. An example is presented which demonstrates the use of the contact model in simulating the foot-ground interaction during the locomotion cycle of a walking machine.

1 Introduction

Simulation of robotic systems invariably requires modeling contact between the robot and the environment. Examples of such contact include foot-ground interaction during the locomotion cycle of a walking machine, finger contact with an object during robotic grasping, and manipulator collision with an unknown object in the workspace. A computationally efficient contact model is needed for rapid simulation of impact, sustained contact under load, and transition to and from contact conditions. This is especially the case in changing topological systems where multiple contacts must be simulated concurrently. In this paper, an efficient contact model is developed using a nonlinear damping term, and several of its important characteristics are presented.

Simulation of impacts or collisions has typically been implemented through application of the rigid body assumption. This assumption requires modeling of impacts as instantaneous events involving impulsive contact forces. Much previous work has used this type of impulsive contact model [1-7].

In the simplest impact case of two objects in pure translation, the rigid body assumption gives

$$v_o = -ev_i, \tag{1}$$

where e is the coefficient of restitution, v_i is the relative velocity before collision, and v_o is the relative velocity after collision. The coefficient of restitution, e, can be defined from Eq. 1 or alternatively by Poisson's Hypothesis [5]. Poisson's Hypothesis breaks impacts into a compression phase and a restitution phase. The coefficient of restitution is then given by

$$e = \frac{P_r}{P_c}, \tag{2}$$

where P_c is the normal force impulse during compression and P_r is the normal force impulse during restitution. Eq. 2 reduces to Eq. 1 for simple cases. In [7], Poisson's Hypothesis is applied to computer animations by modeling a spring at the contact point with two spring constants, k, such that $k_{receding} = e\, k_{compressing}$.

Brach [2] gives an extensive analysis of collisions using the coefficient of restitution with additional coefficients to describe tangential effects. These coefficients are a constant for any given collision, but are not constant across collisions involving different velocities and orientations. This makes the model difficult to use in general simulations.

Wang, Kumar, and Abel [8] note two important physical and mathematical deficiencies of the rigid body assumption which may be overcome by the use of compliant contact models. First, when used with Coulomb friction, cases arise in which no solution or multiple solutions exist. And second, energy conservation principles may be violated in frictional impacts. A compliant contact stress model is proposed in [8], but this may be too complicated for real-time simulation of complex systems involving multiple contacts.

The problems associated with the application of the rigid body assumption motivate the development of compliant contact models for use in simulation. These include the problems noted in [8], the uncertainty of the rigid body coefficients for any particular collision, the difficulty of modeling transitions to and from sustained contact, the neglect of surface compliance, and the need to consider actual contact forces rather than impulsive approximations. This paper proposes the use of a computationally-efficient compliant contact model to overcome many of these problems. The

0-7803-2988-4/96 $4.00 © 1996 IEEE

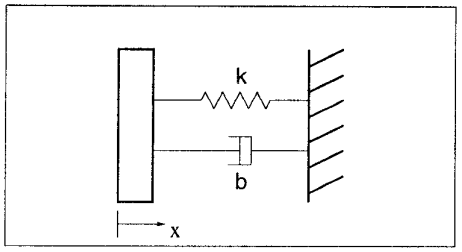

Figure 1: Simple Linear Spring/Damper Model

model uses a nonlinear damping term for improved performance over previous linear models.

In the following section, the nonlinear contact model is presented and motivated over other compliant contact models for rapid simulation. Next, a mathematical formulation of the impact response of the nonlinear contact model is developed to reveal several of its important properties. The section following details several of the performance characteristics of the model. Last, an example of foot contact demonstrates the ability of the model to simulate the foot forces of a walking machine during placement, weight bearing, and lifting.

2 Nonlinear Contact Model

Previous compliant contact models used in simulations have often generated contact forces by simulating a linear spring/damper parallel combination between the objects at the contact point as in Fig. 1 [9, 10]. The interaction force for the contacting objects is then given by the equation

$$f = -b\dot{x} - kx, \tag{3}$$

where x is the penetration depth, b is the damping coefficient (a constant), and k is the spring constant. While computationally simple, this model has many weaknesses [11].

The first weakness is that the contact force is discontinuous at the moment of impact. Before impact, the force is zero. Immediately upon impact, the force due to the spring is still zero, but the damping force is applied instantaneously so that the force steps from 0 to $-b\dot{x} = -bv_i$. Physically, the interaction forces should start at zero and build up over time.

The second weakness is that it permits not only forces due to compression at the contact point but also forces that tend to hold the objects together. In fact, this tensile force is always required just before separation. As the objects are separating, x tends to zero and $\dot{x}$ will be negative and nonzero. The resulting force just before separation will then be $-b\dot{x} = -bv_o$, a tensile force holding the objects together. The effects of this problem may in many cases, however, be lessened by simply setting such forces to zero when they arise.

A final weakness is the dependence of the coefficient of restitution on the mass of the impacting bodies and the lack of dependence on impact velocity. For impact of an object of mass m with a massive object such as the ground, the coefficient of restitution, e, generated by the linear model is given by

$$e = \mathrm{e}^{-b\pi/\sqrt{4mk-b^2}}. \tag{4}$$

This equation can be obtained assuming a damped sinusoidal response of the contact model and no zeroing of tensile contact forces. The coefficient of restitution is an intrinsic property of the material which should not in general depend on mass. However, it should depend on impact velocity. It has been shown that at low impact velocities and for most materials with a linear elastic range [11, 12], the coefficient of restitution can be approximated by the equation

$$e = 1 - \alpha v_i. \tag{5}$$

The coefficient of restitution calculated using the simple linear spring/damper model above shows no dependence of e on v_i, the impact velocity.

A solution to these shortcomings, proposed by Hunt and Crossley [11], is to replace the linear spring/damper parallel combination with a nonlinear one, resulting in a contact force equation of the form

$$f = -(\lambda x^n)\dot{x} - kx^n, \tag{6}$$

where the power n is often close to one and depends on the surface geometry of the impact. In this model, while the spring force is permitted to be nonlinear, the main effect is that the damping is dependent on penetration depth. This makes some sense physically because the damping increases with depth of penetration as more area of the bodies come into contact. In addition, the contact forces evolve continuously upon contact. The dependence of the damping term on x (and also the spring term) causes the force to build up from zero upon contact and return to zero as separation approaches.

Another benefit of this model is that the tensile or sticking forces between the objects do not arise in most situations. It will be shown that in simple impacts there are no sticking forces. In fact, sticking forces only arise when an external force separates the objects at high velocity.

Hunt and Crossley [11] have shown that the coefficient of restitution can be given by Eq. 5 for sufficiently small α and v_i by choosing

$$\lambda = \frac{3}{2}\alpha k. \tag{7}$$

Not only does this nonlinear contact model with the above choice of λ give the desired linear relationship between e and v_i for low impact velocities, but it also exhibits many previously unnoted but important properties at higher impact velocities where the linear relationship does not hold. This will be explored in subsequent sections of the paper.

Choosing $n = 3/2$ in the nonlinear contact model gives results consistent with Hertzian theory for contacting spheres under static conditions [2, 11]. However, the constant n is dependent on the configuration of the impacting bodies which is unknown to a general simulation package. Therefore, using the simple case of $n = 1$, which would apply for impacting flat surfaces [11], would be the simplest approximation.

An alternative contact model has been proposed by Mills and Nguyen [13] which also has some of the same advantages over the simple linear model. This model benefits from the use of a stiff surface component to model collision behavior and a compliant component to model overall behavior. In addition, the contact force varies continuously over time. However, this model requires additional state variables for each contact. This added complexity may be unnecessary or too costly for applications with many contacts. The nonlinear contact model presented here also addresses the major weaknesses of the simple linear spring/damper contact model and maintains great simplicity, requiring only one extra multiplication to calculate contact forces.

3 Mathematical Formulation

In order to further explore the properties of the nonlinear contact model, the equations are developed for the case of a single mass m impacting a massive object such as the earth. For this case, $f = m\ddot{x}$, which when substituted into Eq. 6 leads to Eq. 13 below. Eq. 13 implicitly relates the penetration depth of the mass, x, to the penetration velocity, v, with the direction of penetration being positive for both quantities.

The development is as follows:

$$f = m\ddot{x} = -\lambda x^n \dot{x} - kx^n, \text{ or} \tag{8}$$

$$\ddot{x} = \Lambda x^n \dot{x} + K x^n, \tag{9}$$

where $\Lambda = -\left(\frac{\lambda}{m}\right)$ and $K = -\left(\frac{k}{m}\right)$.

Define $v = \dot{x}$ and $\dot{v} = \ddot{x}$, then

$$\frac{dv}{dx} = \frac{\dot{v}}{\dot{x}} = \frac{\Lambda x^n v + K x^n}{v} = \frac{(\Lambda v + K)\, x^n}{v}, \text{ or} \tag{10}$$

$$\int \frac{v\, dv}{(\Lambda v + K)} = \int x^n\, dx\ . \tag{11}$$

Using the initial conditions $x = 0$ and $v = v_i$ with the integration formula

$$\int \frac{y\, dy}{a + by} = \frac{1}{b^2}\left(a + by - a \ln|a + by|\right) + \text{Const.} \tag{12}$$

leads to:

$$\Lambda v - K \ln|K + \Lambda v| = \frac{1}{n+1}\Lambda^2 x^{n+1} + \Lambda v_i - K \ln|K + \Lambda v_i|\ . \tag{13}$$

It may now be shown that choosing $\lambda = \frac{3}{2}\alpha k$ gives the approximate desired linear relationship between e and v_i for small α and v_i, as expressed in Eq. 5.

From Eq. 13, with $K \ln|K|$ canceled from both sides,

$$\Lambda v - K \ln|1 + (\Lambda/K)\, v| = \frac{1}{n+1}\Lambda^2 x^{n+1} + \Lambda v_i - K \ln|1 + (\Lambda/K)\, v_i|\ . \tag{14}$$

For low loss (αv_i small), $\Lambda v/K$ and $\Lambda v_i/K \ll 1$. The Taylor Series approximation, $\ln|1+\epsilon| = \epsilon - \frac{\epsilon^2}{2} + \frac{\epsilon^3}{3}$ for small ϵ, may then be applied, giving

$$\Lambda v - K\left[\frac{\Lambda v}{K} - \frac{1}{2}\left(\frac{\Lambda v}{K}\right)^2 + \frac{1}{3}\left(\frac{\Lambda v}{K}\right)^3\right] \approx \frac{1}{n+1}\Lambda^2 x^{n+1} + \Lambda v_i - K\left[\frac{\Lambda v_i}{K} - \frac{1}{2}\left(\frac{\Lambda v_i}{K}\right)^2 + \frac{1}{3}\left(\frac{\Lambda v_i}{K}\right)^3\right]\ . \tag{15}$$

For $x = 0$ and $v = -ev_i = -(1 - \alpha v_i)\, v_i$, solving for Λ gives:

$$\Lambda \approx \frac{3\alpha K\,(2 - \alpha v_i)}{2\,(2 - 3\alpha v_i + 3\alpha^2 v_i^2 - \alpha^3 v_i^3)}\ . \tag{16}$$

Since αv_i is small,

$$\Lambda \approx \frac{3}{2}\alpha K, \text{ or} \tag{17}$$

$$\lambda \approx \frac{3}{2}\alpha k\ . \tag{18}$$

This is in fact the same value for λ obtained by Hunt and Crossley in a less rigorous manner [11].

The position, x, can now be solved for explicitly in terms of the velocity, v, for the case when $\lambda = \frac{3}{2}\alpha k$, or equivalently $\Lambda = \frac{3}{2}\alpha K$. This is done by substituting $\frac{3}{2}\alpha K$ for Λ into Eq. 13. The solution, which is a new result, is:

$$x = \sqrt[n+1]{\frac{-2m(n+1)}{9k\alpha^2}}\ \sqrt[n+1]{3\alpha\,(v - v_i) + 2\ln\left|\frac{2+3\alpha v_i}{2+3\alpha v}\right|}\ . \tag{19}$$

Eq. 19 may be used to generate a phase diagram showing penetration velocity vs. penetration. A representative phase diagram is shown in Fig. 2 and will be discussed in the next section.

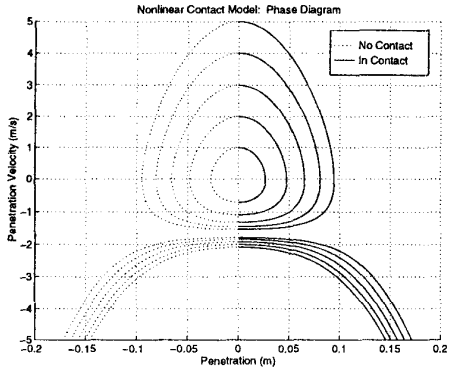

Figure 2: Phase Diagram for $m = 50$ kg, $k = 50$ kN/m, $n = 1$, and $\alpha = 0.4$.

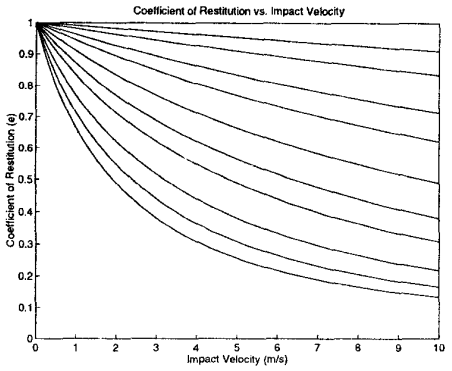

Figure 3: e vs. v_i for $\alpha = 0.01$, 0.02, 0.04, 0.06, 0.1, 0.15, 0.2, 0.3, 0.4, and 0.5 (top to bottom)

A final development, using the relationship of $\lambda = \frac{3}{2}\alpha k$, shows under what conditions the contact force on the mass is positive (inward) or sticky. From Eq. 6,

$$f = -\lambda x^n \dot{x} - kx^n = -\frac{3}{2}\alpha k x^n \dot{x} - kx^n > 0\,. \quad (20)$$

Note since $kx^n > 0$, then

$$-\frac{3}{2}\alpha\dot{x} - 1 > 0\,. \quad (21)$$

Finally,

$$v = \dot{x} < -\frac{2}{3\alpha}\,. \quad (22)$$

Therefore, the contact force on the mass is inward or sticky for $v < -2/(3\alpha)$.

4 Performance Characteristics

4.1 Phase Diagram

The phase diagram [14] for the nonlinear system, which results from using the nonlinear contact model, is shown in Fig. 2. Each contour on the diagram shows how the position and velocity of the mass will vary given initial conditions placing it on the contour and no external forces. For an impact, the contour is entered at x equal 0 and v equal to a positive initial velocity v_i, which causes a positive penetration. The mass follows the contour back around to x equal 0. The dotted part of the contour is included only for completeness in showing the entire phase diagram of Eq. 8. In reality, the equation is not applied for negative penetration (no contact), so only the contours for positive penetration are applicable.

It can be seen in Fig. 2 that the contours converge to a fixed separation velocity as the initial penetration velocity v_i becomes large. This value can be shown to be $v = -\frac{2}{3\alpha}$ from Eq. 19 by setting $x = 0$ and finding the solution for v in the limit as v_i approaches infinity. An intuitive reason for this is that when the velocity reaches $-\frac{2}{3\alpha}$ the spring and damper forces exactly cancel. This causes the mass to return to the surface at that constant velocity since there are no more forces acting on it. Therefore, the two distinct groupings of contours in the phase diagram are always separated by the $v = -\frac{2}{3\alpha}$ line. It was also shown that the contact force is only sticky for $v < -\frac{2}{3\alpha}$. Since the trajectory in a collision never takes v below $-\frac{2}{3\alpha}$, the contact force is never sticky during a collision.

The only way that the system can enter a contour with $v < -\frac{2}{3\alpha}$ is for an external force to actively separate the objects. The system is still stable and dissipative if it gets on one of these contours because the trajectory still takes it back to $x = 0$ with a decreasing velocity. Note that other work in the context of impact control [15, 16] gives additional results concerning the stability analysis.

4.2 Coefficient of Restitution

In this section, the coefficient of restitution produced by the nonlinear contact model is discussed. The variation of e vs. v_i for different values of α is shown in Fig. 3. Note the desired linear relationship in agreement with Eq. 5 for low v_i. The coefficient of restitution decreases with increasing impact velocity and with increasing α. Note also the leveling out trend in e as v_i increases. This is also desirable, as the coefficient of restitution must physically level out before reaching zero so long as the objects still separate. This property for e agrees with that shown by Brach for physical systems [2].

The linear relationship of Eq. 5 is independent of mass, spring constant, and the power n. It is therefore expected that for small αv_i, where the nonlinear contact model approximates Eq. 5, e will be fairly independent of m, k, and n for the nonlinear contact

model. A previously unnoted property of the contact model obtainable with the new analytic solution for the impact response is that e is completely independent of m, k, and n for all impact velocites. This is demonstrated by Eq. 19. In order to solve for e, x is set equal to zero and an expression for the velocity, v, is obtained. When x is set to zero in Eq. 19, the factor composed of the terms under the first radical can be removed, leaving an equation involving only α, v, and v_i. The solution for the final velocity, v, is then independent of m, k, and n so that e is also independent of these. It should be noted that this was an exact solution, so the property holds for all values.

The plots of e vs v_i for various $\alpha's$ in Fig. 3 are therefore valid for any m, k, and n. This is a valuable property which permits m, k, n, and α to be independently set.

4.3 Impact Response Characteristics

The effect of varying α is demonstrated in Fig. 4, which shows how the contact force on the ground varies with the depth of penetration for $m = 1.0$ kg, $k = 10$ kN/m, $v_i = 1.0$ m/s, and $n = 1$. The energy loss is equal to the area within the loop. This results from

$$\triangle Energy = Work = \oint F\,dx. \qquad (23)$$

The energy from the work along the top of the loop is removed and that along the bottom is returned, resulting in the area of the loop being the energy loss. Fig. 4 shows that as α increases, the area of the loop increases indicating the expected increased energy loss. For small α, the plot simply resembles that of a spring. In addition, the increased damping reduces the penetration depth because there is less energy to store in the contact spring.

Fig. 4 also shows the continuous nature of the contact forces, which build up from zero upon impact and smoothly return to zero upon separation. It is also seen that the forces on the ground are never negative (sticky).

Figs. 5 and 6 illustrate how the impact response varies with k, the spring constant. Fig. 5 shows the variation of the contact force with penetration depth for $v_i = 1.0$ m/s, $m = 50.0$ kg, and $\alpha = 0.5$. The area within each hysteresis loop is the same because e, which may also represent energy loss, is independent of k. However, the shape of the hysteresis loop varies with k, as increasing k reduces the penetration depth.

Contact force vs. time is given in Fig. 6 for the same conditions as in Fig. 5. Of interest here is that as k increases, the contact forces become more impulsive. Note also how contact force varies smoothly with time, starting at zero and returning to zero while always remaining compressive.

The effect of varying mass on the impact response

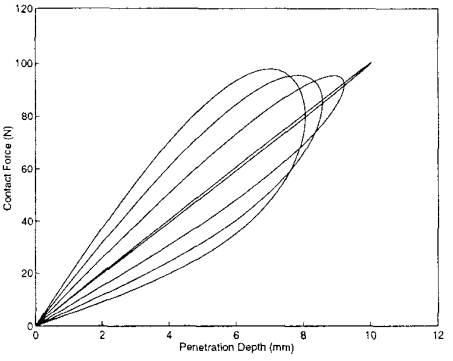

Figure 4: Contact Force vs. Penetration Depth for $\alpha = 0.01$, 0.2, 0.4, and 0.6 s/m (inside out).

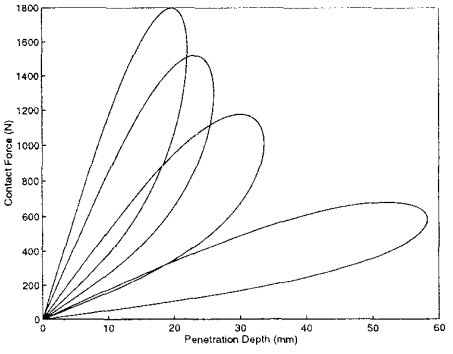

Figure 5: Contact Force vs. Penetration Depth for $k = 10$, 30, 50, and 70 kN/m (bottom to top).

is illustrated in Fig. 7. The area of the hysteresis loop is proportional to the mass, because $\Delta Energy = (1/2)m(v_o^2 - v_i^2) = (1/2)mv_i^2(e^2 - 1)$, which is proportional to m. Fig. 7 also shows that increasing the mass increases the penetration depth, because there is more energy to store in the ground spring. The conditions simulated in Fig. 7 are for $\alpha = 0.5$, $k = 25.0$ kN/m, and $v_i = 0.5$ m/s.

5 Foot Contact Example

A simulation example of the contact model shows the foot-ground interaction of a walking machine during a locomotion cycle. This example illustrates the ability of the contact model to simulate sustained contact conditions, as well as to handle transitions to and from sustained contact.

In this example, the walking machine uses simple position control for foot placement and lift. A constant force is applied to the foot for weight bearing in

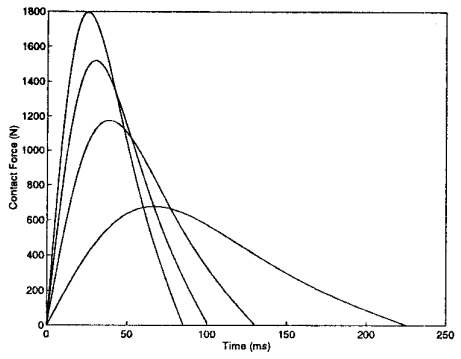

Figure 6: Contact Force vs. Time for k = 10, 30, 50, and 70 kN/m (bottom to top).

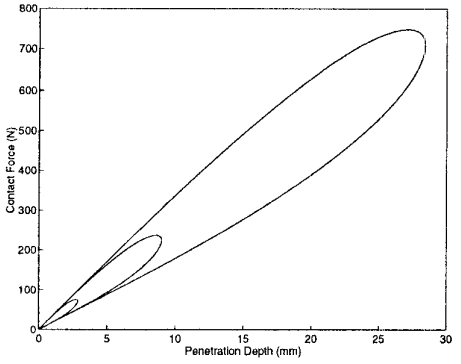

Figure 7: Contact Force vs. Penetration Depth for m = 1, 10, and 100 kg (inside out).

the support phase. The position controller is given as follows:

$$f = K_p(x_d - x), \tag{24}$$

where K_p is the proportional gain, x_d is the desired position, and x is the actual position.

The desired position is determined from the desired velocity profile. At time equal to zero, the desired velocity ramps down from 2 m/s to 0 m/s in 0.1 seconds in preparation for ground contact. This gives the initial parabolic form of x_d seen in Fig. 8. Due to error in the expected ground position, the foot impacts the ground at time 0 with a velocity of 2 m/s, and the desired position turns out to actually be 0.1 m under the ground.

Once the desired velocity is zero, and the foot is assumed to be contacting the ground, the foot begins bearing the weight of the walking machine in a force control mode. At the end of this weight-bearing support phase, the desired velocity jumps to -2 m/s to quickly lift the foot, which causes the ramp seen in the desired position.

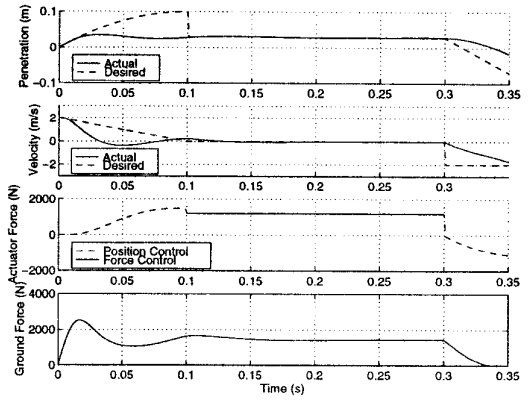

Figure 8: Foot Contact Example: m = 25 kg, α = 0.5 s/m, k = 50 kN/m, and K_p = 20 kN/m.

Analysis of Fig. 8 shows the expected ground interaction. The ground contact prevents the actual position and velocity from tracking the desired position and velocity in the foot placement phase. The positive penetration models the compliance of the ground and leg. The collision also results in a large initial ground force to remove the kinetic energy of the leg and foot. This type of observed behavior in the past motivated the development of reflex controllers to keep forces down to acceptable levels in foot-ground impact [17].

The ground is seen to effectively damp out the oscillations due to the collision. The larger the value of α, the more would be the damping. Note that the ground force is continuous upon impact, and also continuous and outward as the foot is lifted.

This example has demonstrated the use of the nonlinear contact model in sustained contact under load conditions, as well as transitions to and from sustained contact. The form of the response is in agreement with previous results which motivated the development of more complex controllers to handle foot-ground impact. These results support the use of the nonlinear contact model in a variety of contact situations, rather than limiting its use to rebounding impacts.

6 Conclusion

A nonlinear contact model for computer simulation has been presented, and many previously unknown characteristics detailed. These characteristics were shown through a new mathematical formulation of the contact model. Most important of these are the dependence of the coefficient of restitution on impact velocity, ability to independently set parameters, continuous contact forces during contact transitions, and lack of sticking contact forces during collisions. The model has been shown to overcome many problems of the linear contact model, while maintaining the com-

putational simplicity. An example has shown the utility of the model in simulating foot placement, weight bearing, and lift for a walking machine.

Continuing work is being considered using the nonlinear contact model and may include:

- Extending the contact model to include tangential effects.
- Gathering experimental contact force data for closer evaluation of the model.
- Developing a methodology to evaluate model parameters.
- Including the contact model in a general simulation package and demonstrating its computational efficiency for complex systems with multiple contacts.
- Modifying the contact model to include a different damping coefficient for restitution than for compression. Initial exploration has shown that all of the main properties, such as independently setting parameters, still hold while sticking contact forces may be virtually eliminated.

It is hoped that the properties of this contact model will make it useful in a wide range of simulation and control studies.

7 Acknowledgements

Support for this work was provided in part by The Ohio State University and by Grant No. BCS-9311269 from the National Science Foundation to The Ohio State University.

8 References

[1] Y. F. Zheng and H. Hemami, "Mathematical Modeling of a Robot Collision with its Environment," *Journal of Robotic Systems*, vol. 2, no. 3, pp. 289–307, 1985.

[2] R. M. Brach, *Mechanical Impact Dynamics: Rigid Body Collisions.* New York: John Wiley & Sons, 1991.

[3] J. Wittenburg, *Dynamics of Systems of Rigid Bodies.* Stuttgart: B. G. Teubner, 1977.

[4] I. D. Walker, "Impact Configurations and Measures for Kinematically Redundant and Multiple Armed Robot Systems," *IEEE Transactions on Robotics and Automation*, vol. 10, pp. 670–683, October 1994.

[5] Y. Wang and M. T. Mason, "Two-Dimensional Rigid-Body Collisions With Friction," *ASME Journal of Applied Mechanics*, vol. 59, pp. 635–642, September 1992.

[6] J. K. Hahn, "Realistic Animation of Rigid Bodies," *Computer Graphics*, vol. 22, pp. 299–308, August 1988.

[7] M. Moore and J. Wilhelms, "Collision Detection and Response for Computer Animation," *Computer Graphics*, vol. 22, pp. 289–298, August 1988.

[8] Y. T. Wang, V. Kumar, and J. Abel, "Dynamics of Rigid Bodies Undergoing Multiple Frictional Contacts," in *Proc. of the 1992 IEEE International Conference on Robotics and Automation*, (Nice, France), pp. 2764–2769, May 1992.

[9] K. Mirza, M. D. Hanes, and D. E. Orin, "Dynamic Simulation of Enveloping Power Grasps," in *Proc. of the 1993 IEEE International Conference on Robotics and Automation*, (Atlanta, GA), pp. 430–435, May 1993.

[10] H. C. Wong, *Control of a Quadruped Standing Jump and Running Jump Over Irregular Terrain Obstacles.* PhD thesis, The Ohio State University, 1992.

[11] K. H. Hunt and F. R. E. Crossley, "Coefficient of Restitution Interpreted as Damping in Vibroimpact," *ASME Journal of Applied Mechanics*, pp. 440–445, June 1975.

[12] W. Goldsmith, *Impact: The Theory and Physical Behaviour of Colliding Solids.* London: Edward Arnold Ltd., 1960.

[13] J. K. Mills and C. V. Nguyen, "Robotic Manipulator Collisions: Modeling and Simulation," *ASME Journal of Dynamic Systems, Measurement, and Control*, vol. 114, pp. 650–659, December 1992.

[14] D. W. Jordan and P. Smith, *Nonlinear Ordinary Differential Equations.* Oxford: Oxford University Press, 1977.

[15] Y. Shoji, M. Inaba, and T. Fukuda, "Impact Control of Grasping," *IEEE Transactions on Industrial Electronics*, vol. 38, pp. 187–194, June 1991.

[16] P. Akella, V. Parra-Vega, S. Arimoto, and K. Tanie, "Discontinuous Model-based Adaptive Control for Robots Executing Free and Constrained Tasks," in *Proc. of the 1994 IEEE International Conference on Robotics and Automation*, (San Diego, CA), pp. 3000–3007, May 1994.

[17] H. C. Wong and D. E. Orin, "Reflex Control of the Prototype Leg During Contact and Slippage," in *Proc. of the 1988 IEEE International Conference on Robotics and Automation*, (Philadelphia, PA), pp. 808–813, April 1988.